Afsari, N., Sodoudi, F., Taghizadeh Farahmand, F., Reza Ghassemi, M. (2011): Crustal structure of Northwest Zagros (Kermanshah) and Central Iran (Yazd and Isfahan) using teleseismic Ps converted phases. - Journal of Seismology, 15, 2, 341-353

DOP: 10.1007/s10950-011-9227-x

Crustal structure of Northwest Zagros (Kermanshah) and Central Iran (Yazd and Isfahan) using teleseismic Ps converted phases

N. Afsari, 1 F. Sodoudi, 2 F. Taghizadeh Farahmand3 and M. R. Ghassemi4
1) Department of Physics, Parand Branch, Islamic Azad University, Tehran, Iran
2) Helmholtz Center Potsdam, GFZ Research Center for Geosciences, Telegrafenberg 14473 Potsdam, Germany
3) Department of Physics, Qom Branch, Islamic Azad University, Qom, Iran
4) Research Institute for Earth Science, Geological Survey of Iran, Azadi Sq., Meraj. Ave., P. O. Box: 13185-1494, Tehran, Iran.

Abstract

Receiver functions are widely employed to detect P-to-S converted waves and are especially useful to image seismic discontinuities in the crust. In this study we used the P receiver function technique to investigate the velocity structure of the crust beneath the Northwest Zagros and Central Iran and map out the lateral variation of the Moho boundary within this area. Our dataset includes teleseismic data ($M_b \geq 5.5$, epicentral distance from 30° to 95°) recorded at 12 three components short-period stations of Kermanshah, Isfahan and Yazd telemetry seismic networks. Our results obtained from P receiver functions indicate clear Ps conversions at the Moho boundary. The Moho depths were firstly estimated from the delay time of the Moho converted phase relative to the direct P wave beneath each network. Then, we used the P receiver function inversion to find the properties of the Moho discontinuity such as depth and velocity contrast. Our results obtained from PRF are in good agreement with those obtained from the P receiver function modeling. We found an average Moho depth of about 42 km beneath the Northwest Zagros increasing toward the Sanandaj-Sirjan Metamorphic Zone and reaches 51 km, where two crusts (Zagros and Central Iran) are assumed to be superposed. The Moho depth decreases toward the Urmieh-Dokhtar Cenozoic volcanic belt and reaches 43 km beneath this area. We found a relatively flat Moho beneath the Central Iran where, the average crustal thickness is about 42 km. Our P receiver function modeling revealed a shear wave velocity of 3.6 km/s in the crust of Northwest Zagros and Central Iran increasing to 4.5 km/s beneath the Moho boundary. The average shear wave velocity in the crust of UDMA as SSZ is 3.6 km/s which reaches to 4.0 km/s while in SSZ increases to 4.3 km/s beneath the Moho.

Corresponding author: ng_afsari@yahoo.com

Key words: Moho, P receiver function, crustal structure, inversion, Iran, Zagros

1. Introduction

The Iranian plateau is part of the Alpine-Himalayan orogenic belt. The Zagros mountain belt in south-western Iran has resulted from the collision of Arabian Plate with the continental crust of Central Iran after the closure of the Neotethys Ocean (Dewey et al., 1973) (Fig. 1). Geological evidence indicates that the Zagros experienced various tectonic episodes that affected different part of the belt (Falcon 1974; Stöcklin 1977). The present velocity of Arabia with respect to Eurasia is approximately 22 ± 2 mm/yr in the direction N8° ± 5°E at longitude of Bahrain (Vernant et al., 2004). This convergence is accommodated by crustal shortening through fold-and-thrust deformation, and thickening and by lateral displacements of the blocks of Central Iran along major strike-slip faults (Jackson et al., 1995).

The Zagros collision zone comprises three major sub-parallel tectonic elements (Fig. 1). They are, from SW to NE, the Zagros Fold and Thrust Belt (ZFTB), the Sanandaj-Sirjan Metamorphic Zone (SSZ), and the Urmieh-Dokhtar Magmatic Assemblage (UDMA) (Stöcklin, 1968; Ricou et al., 1977). The ZFTB is characterized by a sequence of Paleozoic and Mesozoic shelf sediments that forms a 200-300 km wide simply folded range extending for about 1200 km from eastern Turkey to the Strait of Hormuz (Berberian & King, 1981; Stoneley, 1981). It is bounded to north by the Main Zagros Reverse Fault (MZRF), (Stöcklin 1974; Falcon 1974; Berberian 1995), which is considered to have been the active thrust fault between Arabia and Iran during subduction and before suturing occurred (i.e. Falcon 1974). The MZRF is also characterized as a border between the ZFTB and the SSZ (Stöcklin, 1968, 1974) (Fig. 1). Another major fault in the ZFTB is the NW-SE trending High Zagros Fault (HZF) (Falcon 1974; Berberian 1995), which marks the High Zagros with the highest topography in the region (Fig 1). This part of the Zagros is a narrow thrust belt, which is upthrusted to the southwest along discontinuous different segments of the HZF (M. Berberian & Qorashi 1986). Structural (Tchalenko & Braud, 1974) and seismotectonic (Talebian and Jackson, 2004) observations show that Northwest Zagros accommodates the oblique convergence of Arabia and Eurasia by slip partitioning between shortening within the fold-and-thrust belt, and dextral strike-slip with a NW-SE strike, which more or less follows the trace of the MZRF (see also Fig. 1).

The Sanandaj-Sirjan zone (SSZ) extending in a narrow long (150-200 km wide) belt is the inner crystalline zone of the Zagros orogen and is parallel to the MZRF. The SSZ has undergone various metamorphic episodes during the subduction of the Tethyan Ocean under the Iranian block, the obduction of ophiolites along the MZRF, and the final continental collision (Stöcklin, 1968; Davoudzadeh et al., 1997). During this latest metamorphic episode, the SSZ overthrusted the Zagros sedimentary sequence along the MZRF (Stöcklin, 1968; Agard et al., 2005). The SSZ is bounded to the northeast by the UDMA, which is interpreted as an Andean-type, subduction-related volcanic arc (Berberian & King, 1981). The Central Iranian Micro-Continent (CIMC) is constituted of separated blocks that drifted from Gondwana in the Permian to early-Triassic and subsequently accreted onto Eurasia along the Alborz and Kopet-Dag sutures during the late Triassic closure of the Paleo-Tethy (Stocklin, 1968; Falcon, 1974; Stoneley, 1981).

A few studies have been done on the crustal velocity structure of the Iranian plateau. The depth of Moho and average velocity of seismic waves in the crust are important parameters that characterize the structure of the lithosphere and can often be related to geology, geodynamics and tectonic evolution. Analysis of surface waves dispersion in Iran (Asudeh, 1982b) implied Moho depths of 43-46 km across the Zagros. A refraction profile consisting of sparse recordings along a line from central Iran to the Strait of Hormuz (Giese et al. 1984) showed arrivals of questionable quality identified as Moho reflections and indicated a crustal thickness of 40 km beneath the Central Iran. The only available map of crustal thickness variations for the whole Iranian plateau has been computed from Bouguer anomaly

modeling by Dehghani & Makris (1984). They found a maximum crustal thickness of 50-55 km located right beneath the MZRF and a normal crustal thickness of about 40 km beneath the Central Iran. The more detailed Bouguer anomaly modeling of Snyder & Barazangi (1986) showed a maximum crustal thickness of 55-60 km beneath the MZRF. Hatzfeld et al. (2003) estimated a crustal thickness of 46±2 km from P receiver functions beneath a single station in Central Zagros. More recently Paul et al. (2006, 2010) showed the migrated sections computed from P receiver functions along two profiles (Zagros01, Zagros03) in Central Iran and Northwest Zagros. Their results revealed an average crustal thickness of 42±2 km beneath the ZFTB implying that the crystalline crust of ZFTB has not been significantly thickened by the collision yet. Even though, they showed that crustal thickening starts beneath the north-easternmost part of the ZFTB including the MZRF region and the SSZ (~70 km) along the Central Zagros profile. Even though, they found a thick crust beneath the UDMA and the southern part of the CIMC (~50 km) along the Northwest Zagros profile. They proposed also that the crust of Central Iran overthrusts the crust of Zagros on the MZRF.
This study intends to improve our knowledge on crustal velocity structure beneath the Northwest Zagros and Central Iran. To reach this goal, we use data of three permanent networks of Institute of Geophysics, University of Tehran (IGUT), which are located in the ZFTB, between the ZFTB and CIMC, and in the CIMC. We employ the P receiver function method to constrain the crustal thickness and then apply the 1-D inversion of P receiver function to obtain the shear wave velocity profile beneath each region.

2. Data and methodology

Three different data sets belonging to three telemetry seismic networks of Iran were utilized in this study. All networks are three-component short period and operated by the Institute of Geophysics, University of Tehran (IGUT). The Kermanshah network consists of five stations (DHR, GHG, KOM, LIN and VIS), which are located in Northwest Zagros. Five stations of the Isfahan network (GAR, KLH, PIR, RAM and ZEF) are located between the ZFTB and Central Iran. The Yazd network is located in Central Iran and consists of two stations (CHK, BAF). All stations are equipped with SS-1 seismometers, with a natural frequency of 1 Hz made by Nanometrics. The data were continuously recorded with a sampling rate of 50 samples per second. We used teleseimic events with Mb≥5.5 and epicentral distances between 30°-95° recorded by all stations of Kermanshah, Isfahan and Yazd networks between 2003-2007, 2001-2007 and 2005-2007, respectively. For all networks, most of teleseismic events are limited in the back-azimuth range between 0° and 90°. Short period data were used by several geophysicist to constrain crustal structure (e. g. Zhu, 2000; Ramesh et al., 2005; Sodoudi et al., 2009; Wolbern et al., 2010; Taghizadeh-Farahmand et al., 2010). The methodology used in this paper to calculate P receiver functions in each network, is the same as described by Sodoudi et al. (2006b, 2009). Figure 1 shows the location map of the seismic stations. The names and coordinates of the stations are listed in Table 1.

3. P receiver function Observations

Teleseismic events with relatively high signal-to-noise ratio (>4) have been selected at each station (Fig. 2a). We considered a time window of 110 s in length, starting 20 s before the P onset. To broaden the response of short-period instruments (SS1) into a more useful teleseismic frequency band, the instrument response is deconvolved from the original records. The three components ZNE are then

rotated into the local ray coordinate system LQT using theoretical back azimuth and incidence angle (Fig. 2b). To isolate the P-to-S conversions on the Q component, the L component is deconvolved from the Q component (Fig. 2c). A distance correction (moveout correction) was applied prior to stacking using a reference slowness of 6.4 s/° according to the IASP91 velocity model (Kennett & Engdahl, 1991). Fig. 2 shows the processing steps of P receiver function method for an event recorded at stations VIS and ZEF located in the ZFTB and UDMA respectively. Individual and summed P receiver functions (PRF) for Kermanshah, Isfahan and Yazd networks are presented in Figs. 3a-3c, respectively. The traces for each station are filtered with a band-pass filter of 2-10s and arranged with increasing back azimuth. A clear and coherent P-to-S conversion at the Moho boundary marked as M (Figs. 3a-3c) in the individual traces as well as in the stacked traces is visible in the PRF of all stations. However, the multiple phases from the Moho (PpPs and PpSs, marked with red circles) are mostly very weak. The observed energy at zero time for some stations suggests that either the rotation of the components is not optimal or that shallow local sediments generate some energy. Due to the various structural zones in the study area (Fig. 1), PRFs seem also to be different. For Kermanshah network located in the ZFTB (Fig. 3a), the Moho conversion phase has a delay time ranging between 4.6-5.9s (see also Table. 2). A notable feature, which can be observed underneath almost all stations is the presence of a significant velocity discontinuity at about 1.3 – 2.3s. There is a large difference in the delay time of the Moho conversion phase obtained from the stations of Isfahan network (Fig. 3b). The Moho phase beneath the stations located in the SSZ is significantly delayed. The largest delay time of the Moho phase (~7.1s) can be seen beneath the station GAR located in the SSZ, whereas beneath the UDMA, the Moho phase has the smallest delay time (4.7). Except GAR station, all other Isfahan stations show a clear conversion from the sediments at 0.5-1s. For Yazd network located in Central Iran, the converted Moho phase is clearly observed at 5.5s beneath the BAF station (Fig. 3c). However, there are two phases (at 4.4 & 6.3s), which can be considered as the converted Moho phase beneath the CHK (Fig. 4c). Due to the small number of PRF as well as the low signal-to-noise ratio, the arrival time of the Moho phase can not be easily identified for this station**;** nevertheless, our results are consistent to those obtained by Paul et. al. 2006 in CIMC, near the CHK station. They found two phases at 4.4 s with stronger amplitude and at 6 s and reported about 40 km as Moho depth which is in good agreement with our result (36 km) for CHK station. The clear arrival of the first Moho multiple (at 14s) helped us to estimate the arrival time of the Moho phase. The phase at 4.4s is considered as the conversion at the Moho boundary. The Moho conversion times and their corresponded Moho depths for all stations are listed in Table 2. Moho depths were obtained by using an average crustal P velocity of 6.3 km/s and a Vp/Vs ratio of 1.73 (IASP91). We have to mention, that our obtained Moho depths are the first-order estimate of the velocity structure beneath the Northwest Zagros and Central Iran. This keeps our depth values independent from possible errors of preliminary shear wave velocity models. However, we estimate the deviation to this model to be less than 5%. Therefore, this procedure results in an ±2 km error in the Moho depth determination.

4. P receiver function inversion

Receiver functions are inverted to find the most suitable average shear wave velocity and crustal thickness beneath each seismic station. We used the method, which was described by Kind et al. (1995). The theoretical seismograms are computed for the starting model using the method of Haskell (1962), and then the components are rotated and deconvolved in the same manner as done for the observed traces. The optimal parameters of the model are found by iteratively minimizing the root

mean square difference between the observed and theoretical traces (Kind et al., 1995). We summed Q and L components for each station. For inversion process, a time window between -5 to 30 s was selected. To achieve stability in inversion, both crustal conversions and their strongest multiples are inverted. So regarding the deepest Moho depth beneath all networks, calculated from PRFs and IASP91 model, we chose the time window that all records contain converted phases and their multiples.
The applied inversion method is not unique (Ammon et al 1990), since it tries to find, by definition, models close to the starting model. The method may be successful for different pairs of starting and final models, indicating that the final model depends on the choice of a physically reasonable starting model. In each station, to achieve Moho depth and crustal structure, to improve the convergence of inversion process, inversion was done in two steps. In the first step, we inverted a starting model which were chosen based on the results (P wave velocity and thickness of layers) obtained from previous studies in Zagros and Central Iran (Asudeh 1982b; Giese et al. 1984; Dehghani and Makris, 1984; Snyder & Barazangi 1986; Hatzfeld et al. 2003; Paul et al. 2006; 2010) and our results obtained from PRFs, such as Vp/Vs ratio (Afsari, 2008; Afsari et al., 2010), conversions from the Moho, sedimentary layer and middle crust discontinuities. As initial model, for Yazd and Kermanshah a 60 km and for Isfahan region a 64 km thick crust was chosen which was included different layers with various thicknesses (at least 2 km thick regarding frequency content of signals). After inversion, we selected the models with small root mean square error (less than 0.025s) which their synthetic PRFs had good convergency to observe PRFs then calculated their arithmetic averages. Figure 4 shows two examples of first step for KLH station. In second step, we used these averages as base initial models (see Fig. 5b-B) and repeated inversion process to obtain an optimum model (Fig. 5a). In Kermanshah region, resulted from the first step inversion, a two layered model was inverted in the second step. Even though, three-layered models (three main conversions) were considered for both Yazd and Isfahan regions (Fig. 5b-B). Again, the results with good convergency and low root mean square (less than 0.05 s) were chosen and their arithmetic average was calculated to obtain final crustal model (Fig. 5b-C). It must be noted that during the inversion process, in two steps, both P wave velocity and thickness of layers are adjusted.
Our results show that beneath the Kermanshah region, the thickness of the first layer varies from 9 to 18 km, with S-wave velocity ranging from 3 to 3.5 km/s. Thickness of the second layer varies between 24 to 35 km with S-wave velocity ranging from 3.8 to 4.2 km/s. In Isfahan region, the final crustal model contains three-layers. The thickness of the first layer is estimated to change from 6 to 10 km and the S-wave velocity from 3.1 to 3.3 km/s. The thickness and S velocity of the second layer varies from 14 to 26 km and from 3.4 to 3.7 km/s, respectively. In the last layer the thickness changes from 10 to 30 km and the S-wave velocity varies from 3.8 to 4.0 km/s. In Yazd region, the final model is a three-layered model, in which the thickness of the first layer varies from 6 to 10 km, and its S velocity from 3.1 to 3.6 km/s, respectively. In the second layer the thickness is estimated to vary from 12 to 17 km and the S-wave velocity changes from 3.6 to 4.2 km/s. In the third layer, the thickness and S velocity varies from 17 to 24 km and from 3.9 to 4.4 km/s. Tables 3(a-c) represent the final results of P receiver function inversion for Kermanshah, Isfahan and Yazd regions**.** Also Fig. 6 indicates the average Moho depths, obtained of P receiver functions inversion beneath all three networks located in different tectonic setting.

5. Discussions

We combined our results obtained from PRF and P receiver function inversion to constrain the optimum crustal model beneath the Northwest Zagros and Central Iran. The results of PRF show that

the average Moho depth in northwest of Zagros (Kermanshah region) is about 41 km which is in good agreement with the results obtained by PRF modeling (~42.5). Our results also are in accordance with those obtained from other studies in ZFTB (Paul et al, 2006, 2010). Both RF method and PRF inversion revealed an average thickness of 14km sedimentary layer.
Paul et al. (2010) assumed also a 11 km thick sediment layer beneath the stations in southwest of the MZRF. In Kermanshah region, results of PRFs inversion shows that the crust has a significant thickening (~ 50 km) beneath the station VIS. P receiver function showed also a thick crust of about 50 km beneath this station. We interpret the crustal thickening (~50 km) observed beneath the VIS station as related to the overthrusting system exists there (Berberian, 1995). Beneath the Isfahan region, we found various Moho depths related to the different structural units existed in the area. Results of PRF reveal that in UDMA, average Moho depth is about 47 km but, average Moho depth obtained by PRF modeling is about 43 km. Regarding previous studies in this region (Paul et al, 2006, 2010), 43 km depth is more acceptable. In SSZ, both of methods show that average Moho depth is 51 km. In Isfahan region, the thickest crust was observed beneath the GAR station located on SSZ. Paul et al. (2006) proposed that localized thickening beneath the SSZ is resulted from the overthrusting of the crust of Central Iran on the Zagros crust along the MZRF. The thinnest crust of Isfahan region was found beneath the KLH station located in the UDMA. We found no sharp velocity interfaces beneath this station. No clear layering is due to geological structure beneath the KLH station. Since there Tertiary plutonic rocks are bedded on metamorphic layers; both of these types have not sharp velocity structure as complex as sedimentary rocks. So velocity increase almost monotonically and sharp velocity interfaces are not expected. Similar crustal structure can be seen beneath the ZEF station which is located in the UDMA too. Also we found a relatively flat Moho beneath the Central Iran where, the average crustal thickness is estimated by both methods to be about 42 km which confirms also the results shown by Paul et al. (2006, 2010).

6. Conclusion

We imaged the Moho depth variations and S velocity structure from the records of three seismological networks in Northwest Zagros and Central Iran. We found a relatively flat Moho at 40-43 km depth beneath the whole area including Central Iran and northwest of Zagros except the areas, which have been affected by the overthrusting system of MZRF. Beneath the central part of Kermanshah region a significant crustal thickening to a depth of approximately 50 km (station VIS) was seen. It may show a local effect beneath this part of area, which was also previously reported by Berberian et al. (1995). A local overthrusting system just beneath this station including dipping Moho boundary could be an alternative explanation for the observed feature. Another crustal thickening (56 km) was observed beneath the SSZ, where the crust of Central Iran is assumed to overthrust the crust of the Zagros along the MZRF. We found a thinner crust of 43 km beneath the UDMA in good agreement with the results obtained from previous studies in this region. The average shear wave velocity in the crust of Northwest Zagros and Central Iran was estimated to be 3.6 km/s reaching 4.5 km/s under the Moho boundary. The average shear wave velocity in the crust of SSZ and UDMA is 3.6 km/s which reaches to 4.3 km/s and 4.0 km/s underneath the Moho respectively.

Acknowledgments

We are grateful to the Institute of Geophysics, Tehran University for providing the teleseismic

waveforms. This research was achieved using the software packages SeismicHandler (Stammler, 1993) and GMT (Wessels and Smith, 1998).

References

1) Afsari N, Sodoudi F, Gheitanchi MR, Kaviani A (2010) Moho Depth Variations and vp/vs Ratio in Northwest of Zagros (Kermanshah Region) using Teleseismic Receiver functions. Geoscience 19(**74**): 45-50

2) Afsari N (2008) Crustal structure and azimuthal shear wave velocity anisotropy in Northwest of Zagros (Kermanshah) and Central Iran (Yazd and Isfahan) using teleseismic Ps converted phases. PhD thesis, Science and Research Branch, Islamic Azad University (IAU)

3) Agard P, Omrani L, Jolivet, and Mouthereau F (2005) Convergence history across Zagros (Iran): constrains from collisional and earlier deformation. International Journal of Earth Sciences doi 10.1007/s00531-005-0481-4

4) Berberian M and King GCP (1981) Towards a paleogeography and tectonic evolution of Iran. Can J Earth Sci **18**: 210-65

5) Berberian M (1995), Master blind thrust faults hidden under the Zagros folds: active basement tectonics and surface morphotectonics, Tectonophysics. **241**: 193-224.

6) Dehgani G, and Makris J (1984) The Gravity field and crustal structure of Iran. N Jb Geol Palaont Abh **168**: 215-229

7) Falcon N L (1974) Southern Iran: Zagros mountains. Spec pub Geol Soc London **4**: 199-211

8) Hatzfeld D, Tatar M, Priestley K, and Ghafory-Ashtiany M (2003) Seismological constrains on the crustal structure beneath the Zagros mountain belt (Iran). Geophys J Int **155**: 403-410.

9) Haskell NA (1962) Crustal reflections of plane P and SV waves, J. Geophys. Res, **67**, 4751-4767.

10) Jones CH and Phinney RA (1998) Seismic structure of the lithosphere from teleseismic converted arrivals observed at small arrays in the southern Sierra Nevada and vicinity, California. J Geophys Res **103**: 10065-10090.

11) Kaviani A, Paul A, Bourova E, Hatzfeld D, Pedersen H and Mokhtari M (2007) A strong seismic velocity contrast in the shallow mantle across the Zagros collision zone (Iran). Geophys J Int **171**: 399-410. doi: 10.1111/j.1365-246X.2007.03535.x.

12) Kind R, Vinnik LP (1988) The upper mantle discontinuities underneath the GRF array from P-to-S from converted phases. J Geophys **62**: 138-147

13) Kind R, Kosarve G and Peterson NV (1995) Receiver function at the stations of the German

Regional Seismic Network (GRSN). Geophys J Int **121**:191-202.

14) Kosarev G, Kind R, Sobolev SV, Yuan X, Hanka W, Oreshin S (1999) Seismic evidence for a detected Indian Lithosphere mantle beneath Tibet. Science **283:** 1306-1309.

15) Langston CA, (1977) The effect of planner dipping structure for constant ray parameter. BSSA **67**:1029-1050.

16) McQuarrie N, Stock JM, Verdel C and Wernicke BP (2003) Cenozoic evolution of Neotethys and implications for the causes of plate motions. Geophys. Res Lett **30**:, 2036, doi: 10.1029/2003GL017992.

17) Owens T. J., Zandt, G., and Taylor, S. R., 1984, Seismic evidence for an acient rift beneath the Cumberland Plateau, Tennessee: A detaild analysis of broadband teleseismic P waveform, J. Geophys. Res, **89**, 7783-7795.

18) Paul, A., Kaviani, A., Hatzfeld, D., Vegne, J., and Mokhtari, M., 2006, Seismological evidence for crustal- scale thrusting in the Zagros mountain belt (Iran), Geophys. J. Int., doi: 10.1111/j.1365 24x.2006.02920.x.

19) Paul A, Hatzfeld D, Kaviani A, Tatar M and Pequegnat C (2010) Seismic imaging of the lithospheric structure of the Zagros mountain belt (Iran). Geol Soc London Special Publications 330: 5-18, doi:10.1144/SP330.2

20) Ramesh DS, Wakatsu HK, Watada S, Yuan X (2005) Receiver function images of the central Chugoku region in the Japanese islands using Hi-net data. Earth Planets Space 57(4) 271-280.

21) Ricou LE, Braud J, and Brunn J (1977) Le Zagros Mem. h. ser. Soc Geol Fr **8:** 33-52.

22) Snyder DB, Barazangi M (1986) Deep crustal structure and flexture of the Arabian plate beneath the Zagros collisional mountain belt as inferred from gravity observation. Tectonics **5:** 361-373.

23) Sodoudi F, Kind R, Priestly W, Hanka W, Wylegalla K, Stavrakakis G, Vafidis A, Harjes HP and Bohnhoff M (2006) Lithospheric structure of the Aegean obtained from P and S receiver functions. J Geophys Res **11**: 12307-12330.

24) Sodoudi F, Yuan X, Kind R, Heit B, Sadidkhouy A (2009) Evidence for a missing crustal root and a thin lithosphere beneath the Central Alborz by receiver function studies, Geophysical Journal International. **177**(2): 733-742.

25) Stöcklin J (1968) Structural history and tectonics of Iran: A review, American Association of Petroleum Geologists Bulletin **52**: 1229-1258.

26) Stoneley R (1981) The geology of the Kuh-e Dalnesh area of Southern Iran, and its bearing on the evolution of Southern Tethys. J Geol Soc London **138:** 509-526.

27) Taghizadeh-Farahmand F, Sodoudi F, Afsari N, Ghassemi MR (2010) Lithospheric structure of NW Iran from P and S receiver functions. J Seismology doi: 10.1007/s10950-010-9199-2

28) Tchalenko, J. S., and J. Braud., 1974, Seismicity and structure of the Zagros (Iran): in the Main Recent Fault between 33º and 35º N, Phil. Trans. R. Soc. Lond., **227**: 1-25.

29) Vernant, P., Niloforoushan, F., Hatzfeld, D., Abbassi, M. R., Vigny, C., Masson, F., Nankali, H., Martinod, J., Ashtiani, A., Bayer, R., Tavakoli, F., and Chery, J (2004) Present- day crustal deformation and plate kinematics in the Middle East constrained by GPS measurements in Iran and northern Oman. Geophys. J. Int. **157**: 381-398.

30) Vinnik, L.P (1977) Detection of waves converted from P to Sv in the mantle, Phys. Earth Planet. Inter., **15**, 39-45.

31)Woelbern I, Rümpker G, Schumann A, Muwanga A (2010) Crustal thinning beneath the Rwenzori region Albertine rift, Uganda, from receiver function analysis Int J Earth Sci doi: 10.1007/s00531-009-0509-2.

32) Yuan X, Ni J, Kind R, Mechie J, and Sandivol E (1997) Lithospheric and upper mantle structure of southern Tibet from a seismological passive source experiment. J Geophys Res **102**: 27491-27500

33) Zandt H, and Ammon CJ (1995) Continental crust composition constrained by measurements of crustal Poisson's ratio. Nature **374**: 152-154.

34) Zhu L, and Kanamori H (2000) Moho depth variation in southern California from telesiesmic receiver functions. J Geophys Res **105**: 2969-2980

35) Zhu L (2000) Crustal structure across the San Andreas Fault, southern California from teleseismic converted waves. Earth and Planetary Science Letters **179**: 183-190

Figures Captions:

Fig. 1. Location map of the seismological networks (Kermanshah- Isfahan – Yazd) used in this study. The red box on the topography map shows the location of the study area. Stations are plotted with blue triangles. Red diamonds show cities. The main faults are also shown with thick dark red lines. MZRF: Main Zagros Reverse Fault; HZF: High Zagros Fault; SSZ: Sanandaj-Sirjan Metamorphic Zone; ZFTB: Zagros fold and thrust belt; UDMA: Urumieh-Dokhtar Magmatic Assemblage; CIMC: Central Iranian Micro-Continent.

Fig. 2. P receiver function processing for a teleseismic event recorded in Kermanshah (VIS and ZEF) network which located in ZFTB and UDMA respectively. a) Original teleseismic data signal to noise ratio (> 4). The p-onset is set to be at zero time. b) Restituted data are rotated under the theoretical back azimuth and incidence angle. c) The L component is deconvolved from the Q and T components. d) Moveout corrected P receiver functions. The arrival of the Moho converted phase is shown with the red lines.

Fig. 3. Individual PRF with summation traces for all stations. PRF are plotted equally spaced and sorted by increasing back azimuth (shown in the right). They are filtered with a band-pass filter of 2-10s. The P onset is fixed at zero time. Red dashed line shows the P-to-S converted phase from the Moho (labeled Moho on the summation traces). The predicted arrival times of Moho multiples (regarding IASP91) are also shown with red circles. a) PRF for Kermanshah network. b) Same for Isfahan network. c) Same for Yazd network.

Fig. 4: Two examples of the first step P receiver function inversion for station KLH. Two different initial models are considered (thin lines in the left). Starting and final models are shown by thin and thick lines in the left, respectively. The dotted line in the right is the observed receiver function (Q component), solid lines are synthetic receiver functions for the starting model (thin line at the bottom) and for the final model (thick line of the middle traces). The top trace on the right is the input P signal (L component), which has the normalized amplitude of 1. The amplitude scale of the Q component is also shown.

Fig. 5: a) Two examples of the second step receiver function inversion for station KLH. Two different initial models are considered. b) Inversion steps to find the most suitable average shear wave velocity and crustal thickness for station KLH. A) Initial models for first step inversion (light blue lines) and their average model (dark blue line). Different simple models are considered. Velocities and thicknesses are based on the results obtained from previous studies in this region. B) Results of first step inversion (light blue lines) and their average model (dark blue line). Note that only convergent final models with a root mean square error less than 0.025 are considered. The average of them regarding the number of P-to-S conversions seen in Fig. 2 is considered as the initial model for the second step inversion. C) Results of second step inversion (light blue lines) and their average model (dark blue line), which presents the final model for station KLH. Only convergent models with a small root mean square error (less than 0.05s) are considered.

Fig. 6: Sketch map of the study area with the average Moho depths, indicated by solid color circles.

Figures:

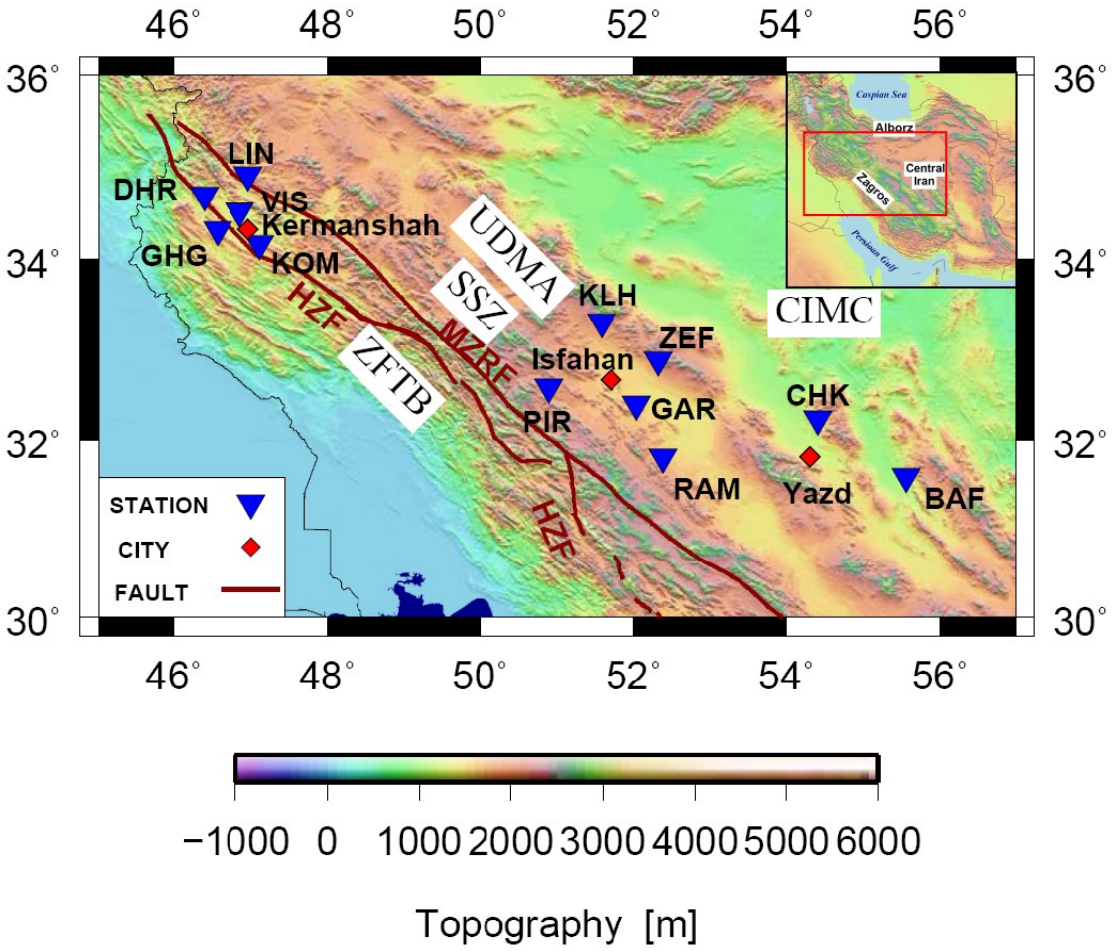

Fig. 1.

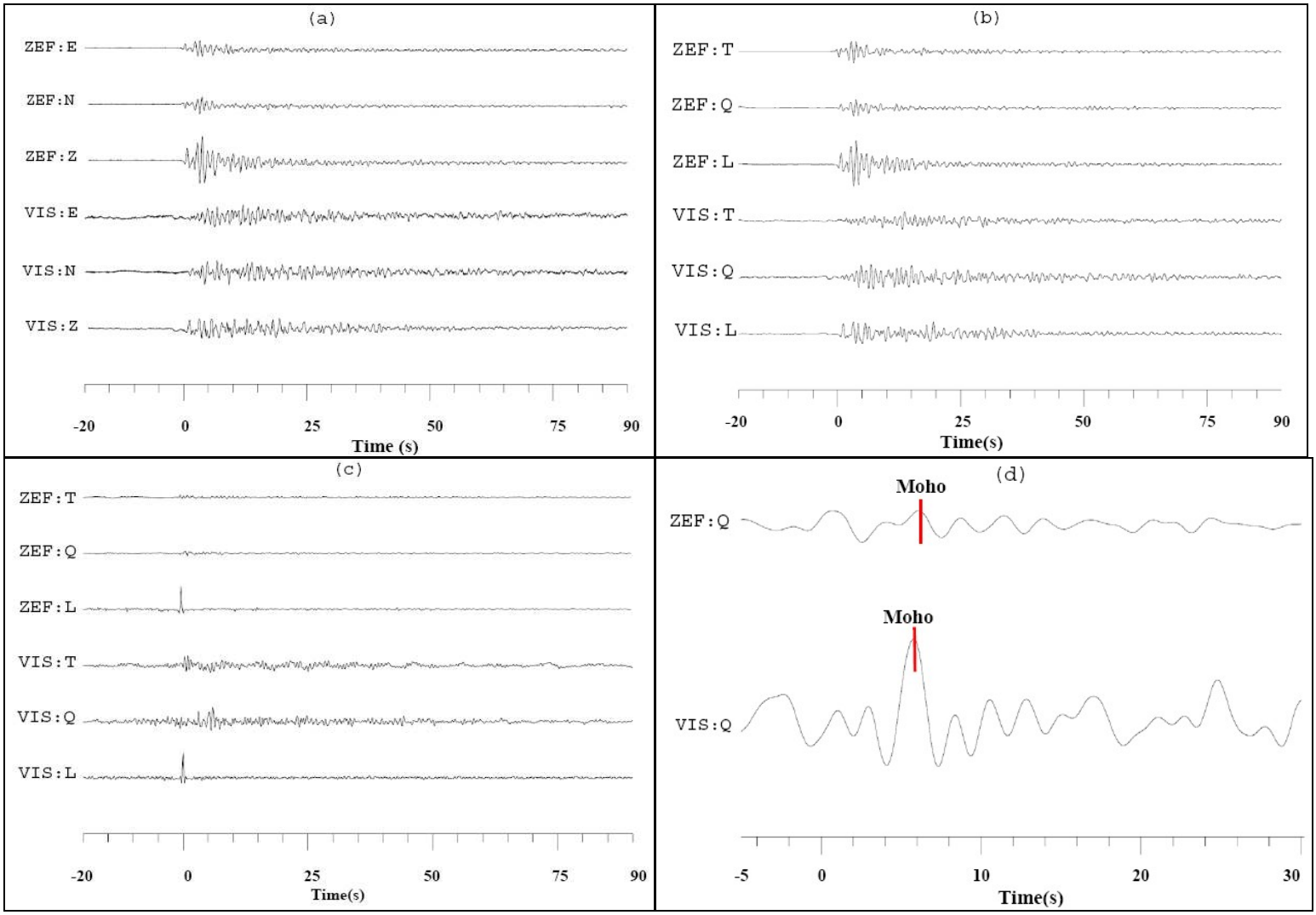
(a)
ZEF:E
ZEF:N
ZEF:Z
VIS:E
VIS:N
VIS:Z
-20
0
25
50
75
90
Time (s)
(b)
ZEF:T
ZEF:Q
ZEF:L
VIS:T
VIS:Q
VIS:L
-20
0
25
50
75
90
Time(s)
(c)
ZEF:T
ZEF:Q
ZEF:L
VIS:T
VIS:Q
VIS:L
-20
0
25
50
75
90
Time(s)
(d)
Moho
ZEF:Q
Moho
VIS:Q
-5
0
10
20
30
Time(s)

Fig. 2.

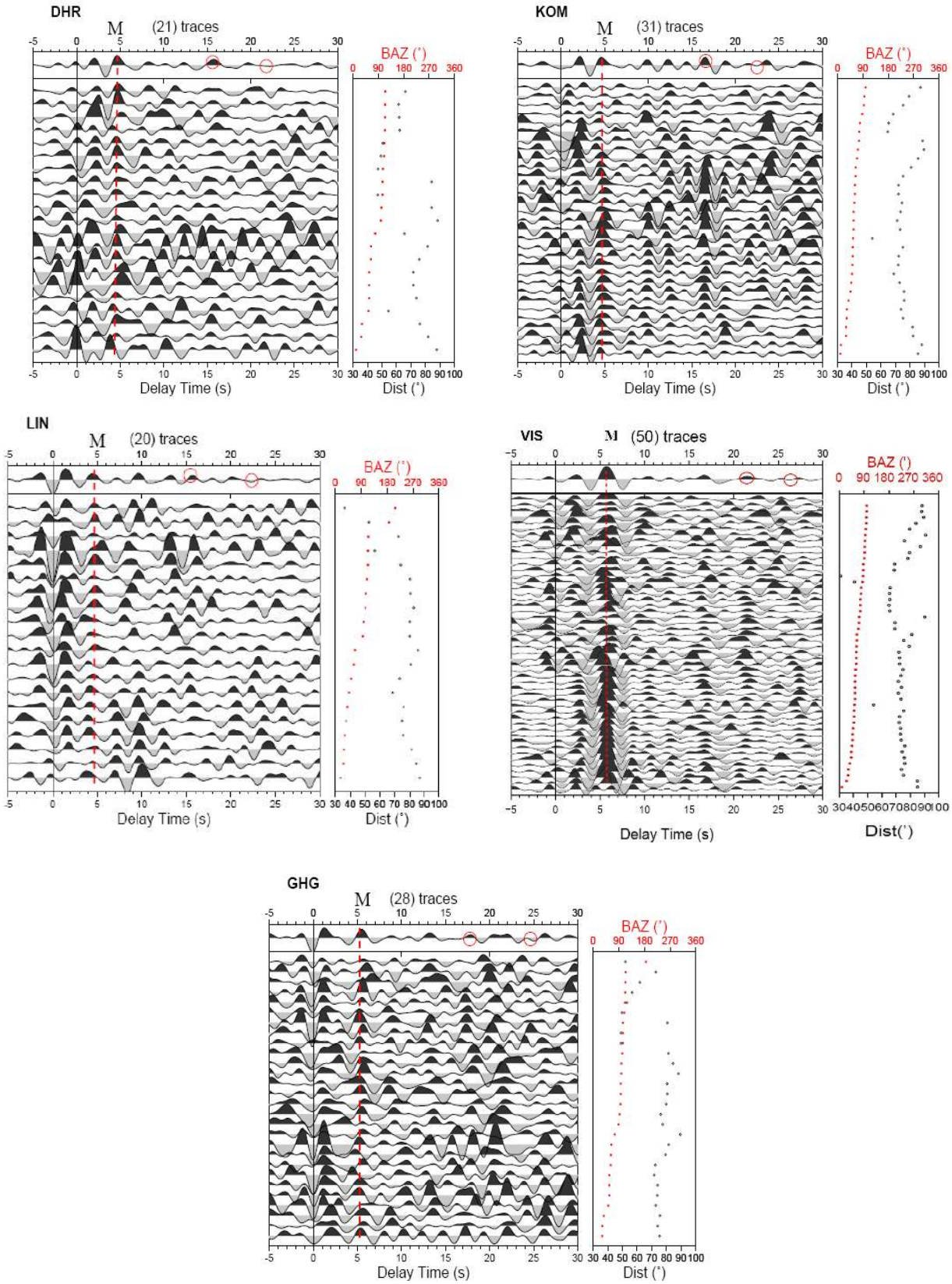
DHR
M
(21) traces
BAZ (°)
Delay Time (s)
Dist (°)
KOM
M
(31) traces
BAZ (°)
Delay Time (s)
Dist (°)
LIN
M
(20) traces
BAZ (°)
Delay Time (s)
Dist (°)
VIS
M
(50) traces
BAZ (°)
Delay Time (s)
Dist(°)
GHG
M
(28) traces
BAZ (°)
Delay Time (s)
Dist (°)

Fig. 3a.

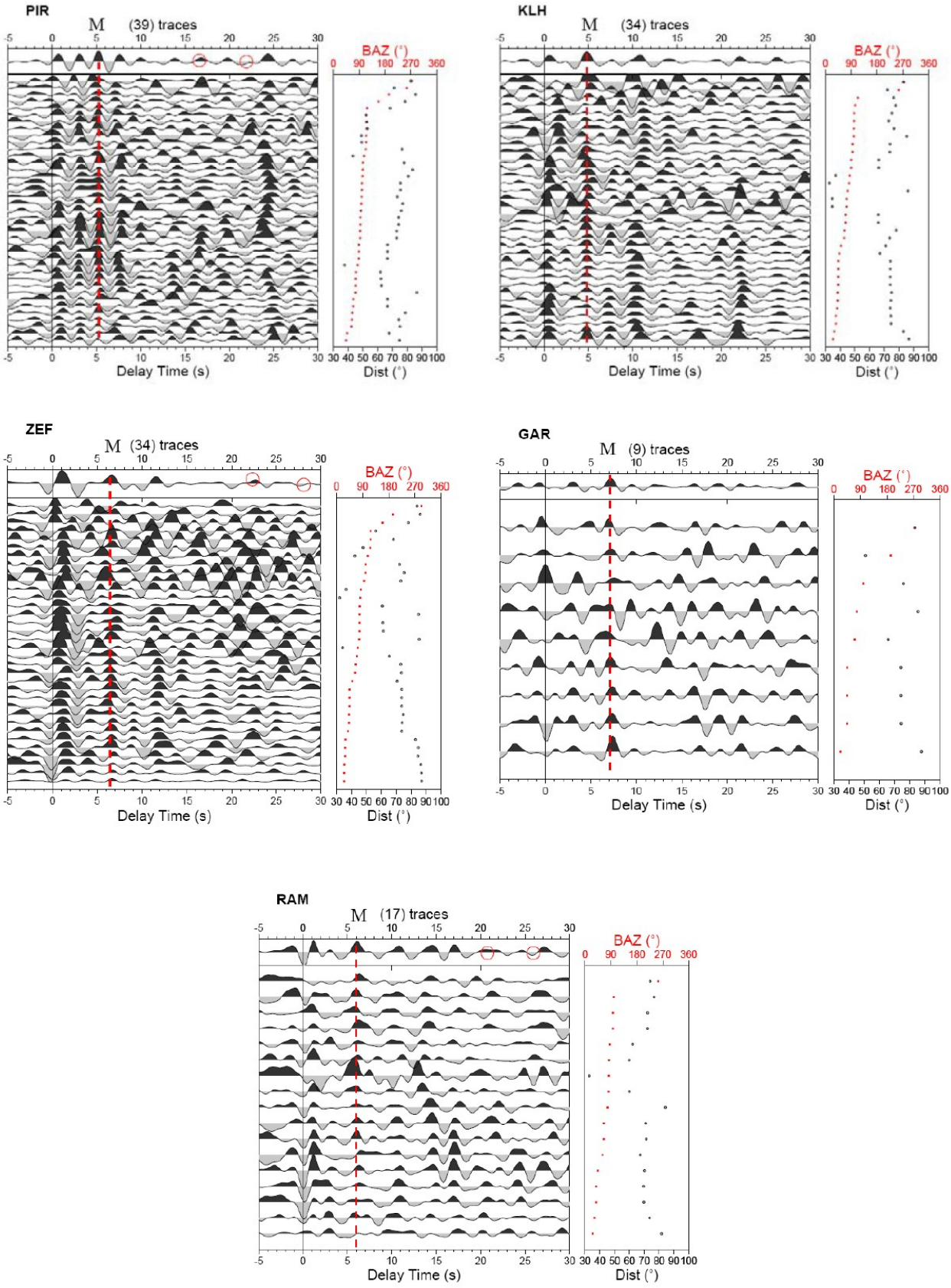
PIR
M (39) traces
BAZ (°)
Delay Time (s)
Dist (°)
KLH
M (34) traces
BAZ (°)
Delay Time (s)
Dist (°)
ZEF
M (34) traces
BAZ (°)
Delay Time (s)
Dist (°)
GAR
M (9) traces
BAZ (°)
Delay Time (s)
Dist (°)
RAM
M (17) traces
BAZ (°)
Delay Time (s)
Dist (°)

Fig. 3b.

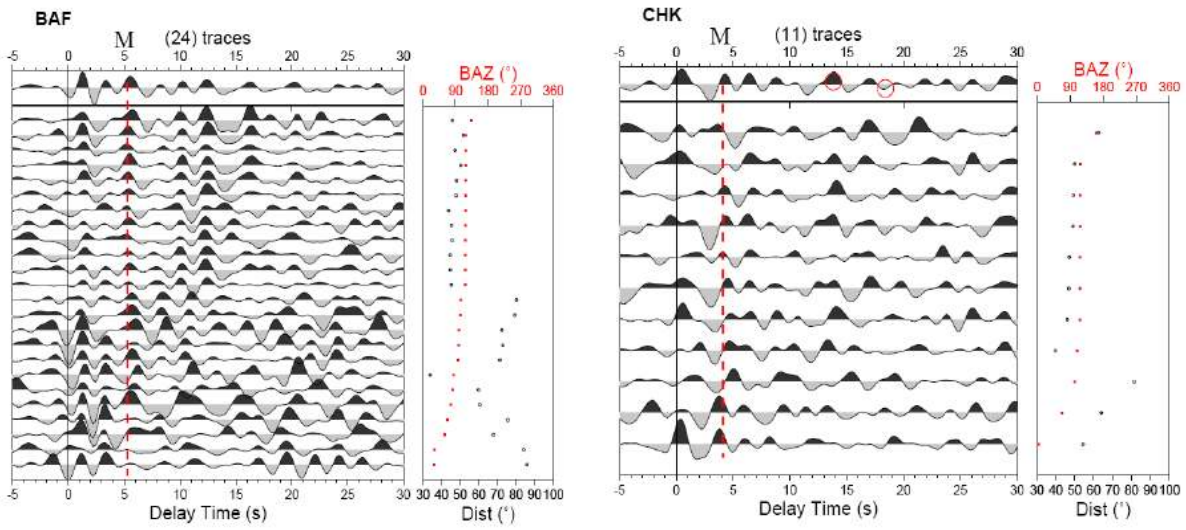
BAF
M
(24) traces
BAZ (°)
Delay Time (s)
Dist (°)
CHK
M
(11) traces
BAZ (°)
Delay Time (s)
Dist (°)

Fig. 3c.

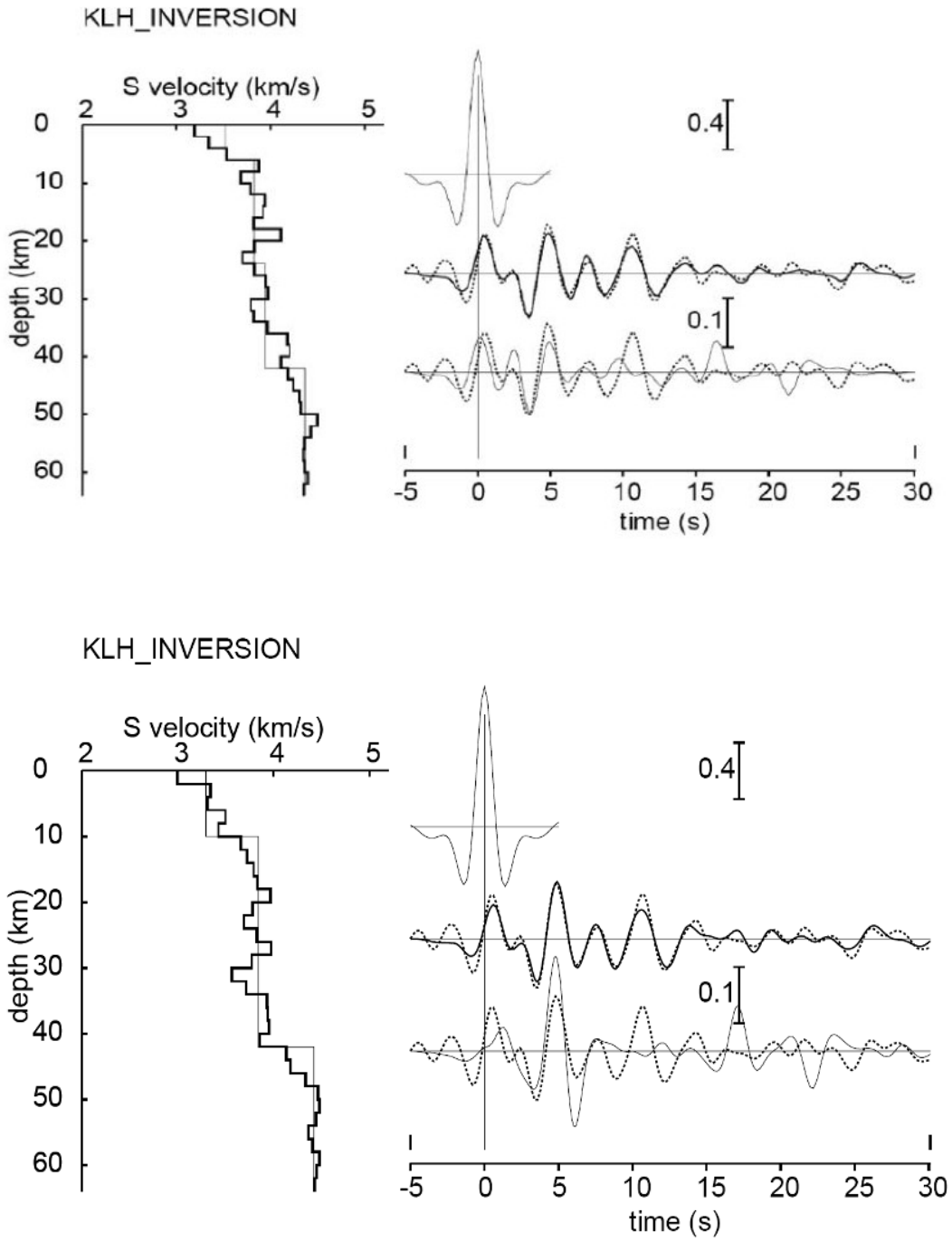
KLH_INVERSION
S velocity (km/s)
2
3
4
5
0
10
20
30
40
50
60
depth (km)
0.4
0.1
-5
0
5
10
15
20
25
30
time (s)
KLH_INVERSION
S velocity (km/s)
2
3
4
5
0
10
20
30
40
50
60
depth (km)
0.4
0.1
-5
0
5
10
15
20
25
30
time (s)

Fig. 4.

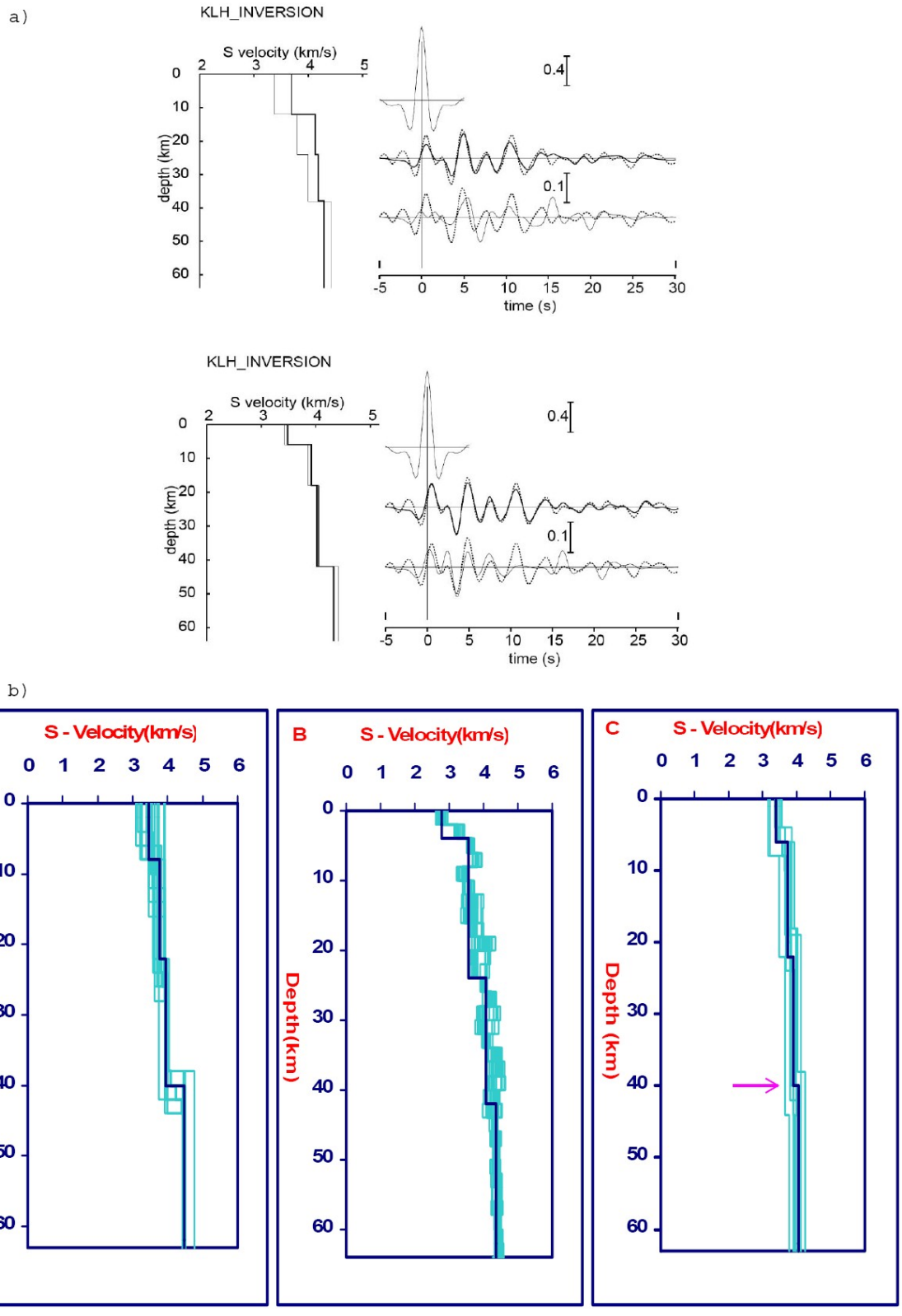
a)
KLH_INVERSION
S velocity (km/s)
depth (km)
0.4
0.1
time (s)
KLH_INVERSION
S velocity (km/s)
depth (km)
0.4
0.1
time (s)
b)
A
S - Velocity(km/s)
Depth(km)
B
S - Velocity(km/s)
Depth(km)
C
S - Velocity(km/s)
Depth (km)

Fig. 5.

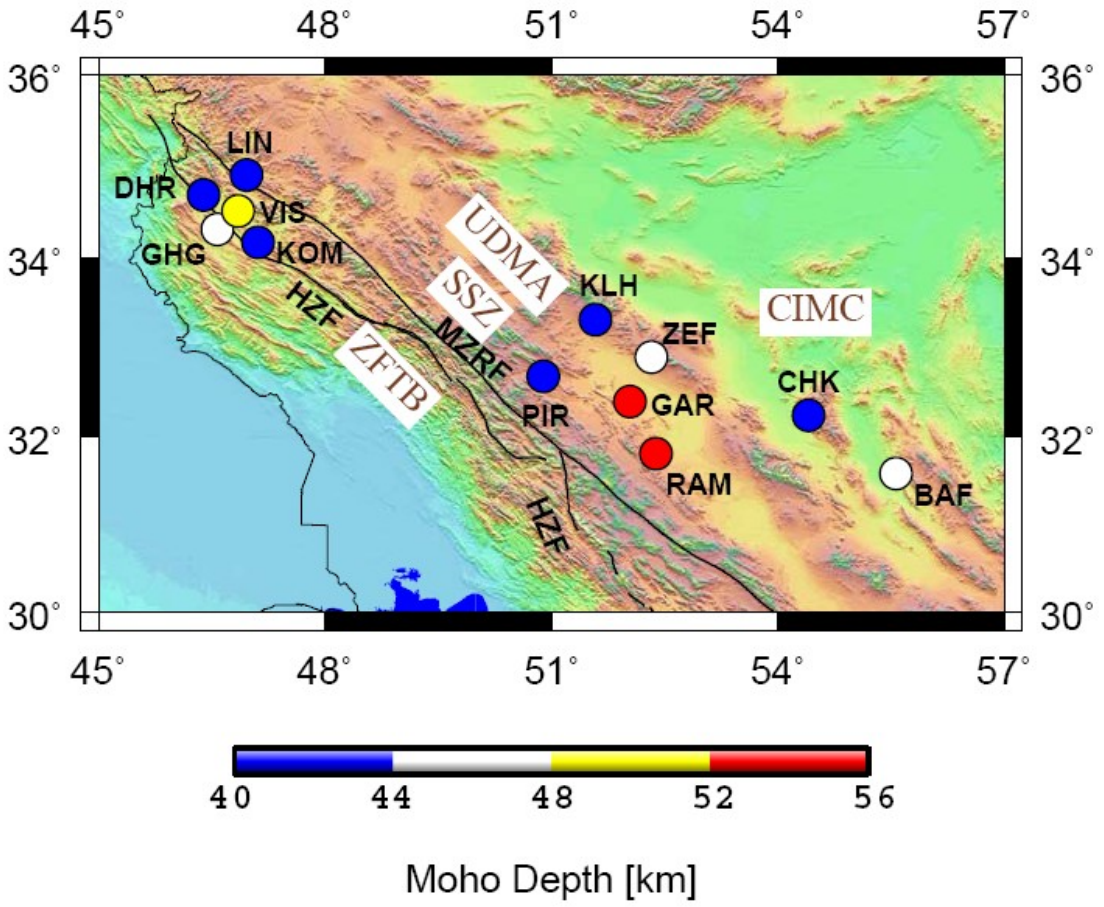
45°
48°
51°
54°
57°
36°
34°
32°
30°
LIN
DHR
VIS
GHG
KOM
HZF
ZFTB
UDMA
SSZ
MZRF
PIR
KLH
ZEF
GAR
RAM
CIMC
CHK
BAF
HZF
40
44
48
52
56
Moho Depth [km]

Fig. 6.